Citation (APA)
Nguyen, H., Korving, L., Prot, T., Cazalet, D., van Veelen, H. P. J., Roy, S., Belloni, C., Dugulan, A. I., & van Loosdrecht, M. C. M. (2026). Full-scale conversion of a wastewater treatment plant from biological to chemical phosphorus removal for vivianite formation. *Water Research*, *305*, Article 126510.
https://doi.org/10.1016/j.watres.2026.126510

Water Research 305 (2026) 126510

Contents lists available at ScienceDirect

Water Research

journal homepage: www.elsevier.com/locate/watres

Full-scale conversion of a wastewater treatment plant from biological to chemical phosphorus removal for vivianite formation

Ha Nguyen[a,b,*], Leon Korving[a], Thomas Prot[a], Damien Cazalet[c], H. Pieter J. van Veelen[a], Samarpita Roy[b], Carlo Belloni[a], A. Iulian Dugulan[d], Mark C.M. van Loosdrecht[b]

[a] Wetsus, European Centre of Excellence for Sustainable Water Technology, Oostergoweg 9, Leeuwarden, MA, 8911, the Netherlands
[b] Department of Biotechnology, Delft University of Technology, Van der Maasweg 9, Delft, HZ, 2629, the Netherlands
[c] Veolia Wasser Deutschland GmbH, Walter-Köhn Str. 1a, Leipzig, 04356, Germany
[d] Department of Radiation Science and Technology, Delft University of Technology, Mekelweg 15, Delft, JB, 2629, the Netherlands

HIGHLIGHTS

- Full-scale shift to from biological chemical P removal enabled vivianite production.
- 90 % of digester P converted to vivianite when Fe/P raised from 0.5 to 1.6. Vivianite formed mainly in the waterline, not in the digester.
- Dewatered sludge dry matter increased by 25 % with iron dosing due to vivianite formation. Effluent total P decreased 86 %, COD decreased 36 %, biogas H_2S nearly eliminated.
- Microbial shifts were reversible; PAOs remained largely stable.
- Iron dosing in primary thickener led to Fe reduction and recirculation to waterline.

GRAPHICAL ABSTRACT

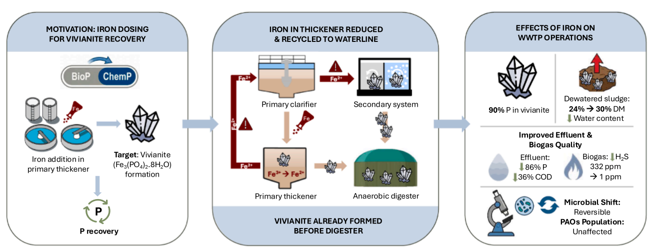

ARTICLE INFO

Keywords:
Vivianite
Phosphorus recovery
Biological P removal
Chemical P removal
Polyphosphate-accumulating organisms

ABSTRACT

This study evaluates the operational impacts and vivianite formation potential of converting a full-scale wastewater treatment plant from Enhanced Biological Phosphorus Removal (EBPR) to Chemical Phosphorus Removal (CPR) with the aim of producing vivianite-rich sludge as a prerequisite for downstream phosphorus recovery in the form of vivianite. By increasing the Fe/P molar ratio in digested sludge from 0.5 to 1.6, up to 90 % of sludge phosphorus was bound as vivianite. Although the additional iron was dosed into the primary sludge line to target vivianite formation in the digester, substantial vivianite formation may have occurred mainly in the secondary system before anaerobic digestion. The transition to CPR improved effluent quality (86 % lower P and 34 % lower COD), reduced biogas H_2S levels from 332 ppm to 1 ppm, and increased dewatered cake dry matter from 24 % to 30 %. Mass balances indicated that dosing iron into the primary thickener triggered substantial reduction of Fe^{3+} to Fe^{2+}, causing iron recirculation to the influent and possibly impairing primary settling. Microbial analysis showed pronounced but reversible shifts in community structure, while

* Corresponding author.
E-mail address: vietha3112@gmail.com (H. Nguyen).

https://doi.org/10.1016/j.watres.2026.126510
Received 9 April 2026; Received in revised form 6 July 2026; Accepted 15 July 2026
Available online 16 July 2026

Polyphosphate-Accumulating Organisms (PAOs) remained stable before and after the return to EBPR operation. For future implementation, maintaining waterline iron dosing for effluent P control while dosing only the additional iron required for vivianite formation directly into the digester may improve process stability, but this strategy requires site-specific testing.

1. Introduction

At wastewater treatment plants (WWTP), phosphorus (P) removal is achieved through Enhanced Biological Phosphorus Removal (EBPR/bioP) or Chemical Phosphorus Removal (CPR/chemP). EBPR stores P biologically in polyphosphate-accumulating organisms (PAOs) (van Loosdrecht et al., 1997), whereas CPR precipitates P using iron or aluminium salts (Korving et al., 2019; Wilfert et al., 2015). Regardless of the removal strategy, over 90 % of influent P accumulates in sewage sludge, making sludge the primary target for P recovery (Egle et al., 2016). In EBPR systems, struvite precipitation from digested sludge liquors is a mature recovery technology, but typically recovers only 15–30 % of influent P due to limited P release during digestion and strong binding to biomass or metal-associated phases (Wilfert et al., 2015).

An emerging alternative is vivianite ($Fe_3(PO_4)_2 \cdot 8H_2O$) recovery. Vivianite naturally forms under anaerobic conditions in iron-rich sludge and can bind a large fraction of total phosphorus given sufficient iron dosing (Prot et al., 2020; Wilfert et al., 2018). A recent pilot study has demonstrated that magnetic separation of vivianite (ViviMag®) can recover up to 60 % of the total influent phosphorus (Wijdeveld et al., 2022). Furthermore, this technology has proven to be robust, performing effectively across a range of sludge dry matter (DM) contents as well as varying vivianite concentrations and particle sizes (Nguyen et al., 2024). However, this route is limited in EBPR plants, where iron dosing is intentionally kept low to maintain biological performance. Therefore, converting EBPR systems to CPR by increasing iron input could be considered a strategy to promote phosphate recovery as vivianite.

Economic and regulatory drivers significantly accelerate vivianite recovery. German legislation (AbfKlärV, 2017) mandates phosphorus recovery by 2029 for WWTPs above 100 000 PE and by 2032 for WWTPs above 50 000 PE, typically via off-site treatment or mono-incineration with subsequent extraction from ash, unless the phosphorus content is below 20 g P/kg DM. Implementing recovery technologies like ViviMag® directly at the WWTP can reduce residual phosphorus below this threshold while avoiding the high costs of downstream incineration, which are estimated at 320–480 EUR per ton DM (Könemann et al., 2024).

We investigated a full-scale EBPR municipal WWTP in Schönebeck, Germany. This plant was operated under CPR conditions for over 8 months through targeted iron dosing in the sludge line to form vivianite in the digester, with the aim of increasing vivianite formation in the produced sludge as a preparation step for downstream ViviMag® recovery. The magnetic separation step (ViviMag®) itself was not evaluated in the present study, but has been addressed in separate recovery-focused studies (Grönfors et al., 2022; Nguyen et al., 2024). This study created a unique case study to monitor, for the first time, the transition from bioP to chemP operation and its reversal over one year. By monitoring the process before, during, and after iron dosing, we evaluated vivianite formation in the digester. Additionally, this allowed us to assess the potential impact of iron dosing on the microbial community. This study addresses the key question of whether converting bioP to chemP is a practical and effective approach to meet future phosphorus recovery requirements.

2. Methods

2.1. WWTP and iron dosing

The study was conducted at a municipal WWTP in Schönebeck, Germany (*Abwasserentsorgung Schönebeck GmbH*), designed for approximately 90 000 population equivalents (PE) (Fig. 1). The plant is underloaded and operates at a load of 60 000 – 70 000 PE with an average influent flow rate of 9 000 m^3/day. The plant has primary settling, after which the primary effluent flows to the secondary treatment with an activated sludge process for biological nitrogen and phosphorus removal. This secondary system consists of an anaerobic tank followed by three consecutive anoxic-oxic tank pairs in series. The sludge retention time (SRT) of the secondary system is about 25 days. To control odors and maintain a good effluent phosphate quality, some ferric salt was added at the WWTP inlet and before the secondary clarifier. Both primary and secondary sludges were thickened and then fed to an anaerobic digester with an SRT of 20 days. Along with the two sludges, 25 % of the digester feed consisted of a co-substrate composed of fat, oil, and grease collected from nearby restaurants. From the digester, the sludge moves to the dewatering unit and the dewatering centrate is recycled back to the secondary treatment system.

To promote vivianite formation in the sludge, additional iron was dosed into the primary sludge pumping station from 13 April 2022 until 31 December 2022 (Fig. 2), increasing the Fe/P molar ratio in the digested sludge from 0.5 to 1.6. This dosing location was selected mainly for practical reasons. Since the objective was to increase the iron load entering the anaerobic digester, dosing in the sludge line was preferred over additional dosing in the water line. Direct dosing to the digester would have provided the most targeted route, but no suitable dosing point was available at the plant. The primary sludge line was therefore selected as the most practical available location, as it provided relatively direct access to the digester through the sludge line. The original dosing points were also kept active, but during the test period, the type of iron salt was changed from $FeClSO_4$ to $FeCl_3$. This change was made to reduce sulphide formation in the digester, as sulphide competes with phosphorus for iron binding, limiting vivianite formation (Prot et al., 2020). After the increased iron dosing period, the WWTP returned to its original operation from January 2023.

2.2. Sampling campaign

Samples were collected weekly from various locations (Fig. 1) across the plant during the intensive monitoring period from 05/04/2022 to 31/12/2022, corresponding to approximately 39 weeks. On-site measurements were conducted immediately after sampling for phosphate, soluble and total chemical oxygen demand (COD) and soluble Fe^{2+} using Hach Lange test kits (Hach Company, Loveland, Colorado), with the soluble fraction measured by passing the liquid through the 0.45 μm filter. Because Fe^{3+} has very low solubility at near-neutral pH and readily hydrolyses to ferric hydroxides, the filtered soluble iron fraction was operationally interpreted as mainly Fe^{2+}. Portions of these samples were frozen and transported to the laboratory for analysis of total phosphorus, total iron, and for determining total and volatile solids (TS and VS). To assess the status of the microbial community in the secondary system, sludge samples were collected bi-weekly from the first anaerobic tank in the secondary system and were also stored frozen for sequencing at −80 °C.

Global parameters were obtained directly from the WWTP's SCADA system. These parameters included flow rates, aeration levels, polymer dosing, nitrogen fractions in both the secondary treatment and effluent, biogas production, TS in the dewatered cake, and the quantity of disposed sludge.

Before increased iron dosing started, two samples were collected on 05/04/2022 and 12/04/2022, to establish the original operational status of the WWTP. After the extra iron dosing ended on 31/12/2022, the primary focus shifted to monitoring microbial changes. Samples were taken only from the primary settler outlet, the secondary thickened sludge, and the dewatering centrate. Microbial analysis continued in the anaerobic tank of the secondary system, while sampling of other locations was discontinued. The last sample was collected on 11/04/2023, approximately 53 weeks after the start of the monitoring campaign.

2.3. Analyses

2.3.1. Elemental compositions

Sludge samples, including primary, secondary thickened, and digested sludge, were dried at 105 °C and subsequently ground prior to microwave digestion. A separate aliquot of the dried sludge was incinerated at 550 °C to determine VS. For waterline samples, approximately 10 ml was used per digestion. All samples were digested using a Milestone Ethos Easy microwave digestion system fitted with an SK-15 high-pressure rotor. Each sample was placed in a Teflon vessel with 10 ml of 69 % ultrapure HNO_3. The digestion process involved heating the mixture to 200 °C for 15 min, holding at that temperature for another 15 min, followed by a cooling period of about one hour.

After digestion, the samples were diluted and analyzed using Inductively Coupled Plasma Optical Emission Spectroscopy (ICP-OES) with a Perkin Elmer Optima 5300 DV instrument. An ESI-SC-4 DX autosampler was used, and data acquisition was managed through the WinLab32 software. A 10 mg/l Yttrium solution served as the internal standard, and 2 % HNO_3 was used as the rinsing solution.

2.3.2. Vivianite quantification

Vivianite identification was carried out through Mössbauer spectroscopy in combination with elemental analysis by ICP-OES. Prior to analysis, the sludge samples were centrifuged and dried at ambient temperature inside an anaerobic chamber and then ground. Spectra were recorded at room temperature (295 K) and low temperatures (4.2 and 20 K) using a conventional constant-acceleration Mössbauer spectrometer equipped with a $^{57}Co(Rh)$ radiation source. Velocity calibration was performed using an α-Fe reference foil, and spectral fitting was conducted using the MossWinn 4.0 software (Klencsár, 1997). The details of the fitting can be found in the Supplementary section S1.

2.3.3. Microbial community

Biweekly, 500 ml of sludge from the first anaerobic tank in the secondary system was frozen and stored at −80 °C for DNA extraction. To prepare for extraction, the samples were thawed overnight. DNA was extracted using the DNEasy PowerSoil Pro Kit (QIAGEN (50)), following the manufacturer's protocol with a modification to the lysis procedure. Instead of a continuous 10-minute lysis, the protocol was changed into alternating one-minute bead-beating with one-minute incubation on ice, repeated ten times. This modified approach aimed to minimize DNA degradation or denaturation during cell lysis. Mechanical disruption of cells was carried out using the Mini BeadBeater by BioSpec Products.

Extracted DNA was quantified using the Qubit 1X dsDNA Broad Range Assay and measured on a Qubit 4 Fluorometer (Thermo Fisher Scientific). Prior to measurement, DNA samples were diluted with Milli-Q water to ensure the concentrations fell within the assay's standard range. Purity assessment was performed spectrophotometrically using a Synergy HTX Multi-Mode Reader (Thermo Fisher Scientific). For each sample, 1 µL of DNA extract was pipetted in duplicate onto a microplate. Purity was evaluated based on absorbance ratios: A260/A280 for protein contamination (ideal >1.8) and A260/A230 for contaminants such as salts and organic substances (optimal 2.0–2.2). A low A260/A230 ratio may indicate the presence of guanidine hydrochloride, a component of the lysis buffer, which does not interfere with downstream molecular analyses. The extracted DNA samples were subsequently sent to Novogene (China) for 16S rRNA gene sequencing targeted for the V4-V5 regions to profile microbial community composition.

DNA sequence data were processed using QIIME2 (v.2022.2) (Bolyen et al., 2019) and denoised using DADA2. Microbiome profiles were then imported with *phyloseq* v.1.40.0 (McMurdie and Holmes, 2013) in R Statistical Software (v.4.2.0) (R Core Team). The "general core" microbes comprising amplicon sequence variants (ASVs) with prevalence in at least 50 % of samples with a mean relative abundance >0.1 % were filtered according to Dueholm et al. (2022). Genus abundances from SILVA database were calculated by agglomerating ASVs to visualize seasonal patterns. Constrained analysis of principal coordinates was performed using *capscale* from the vegan package (v.2.6–4) (Oksanen

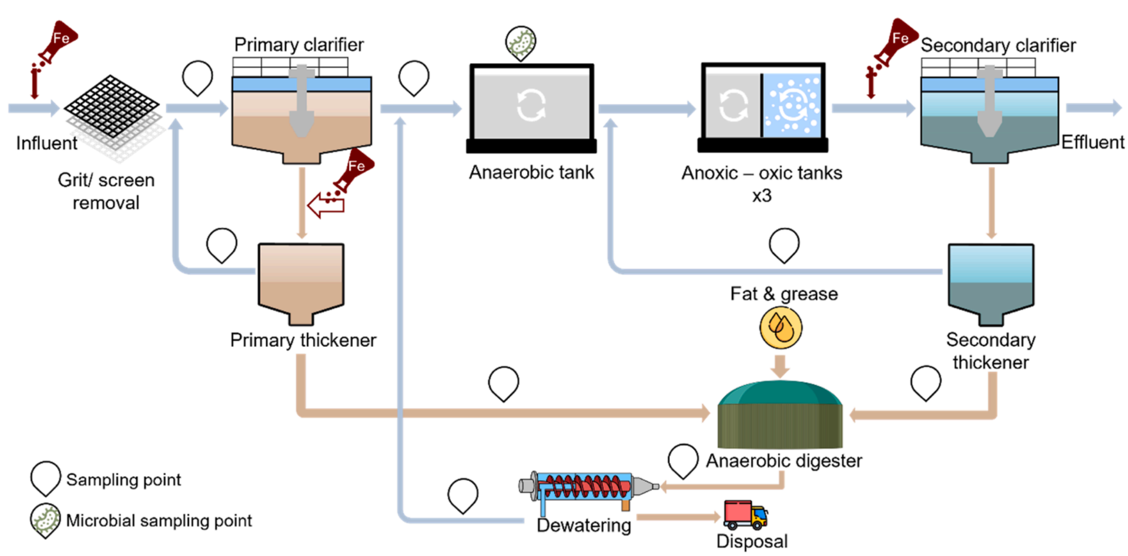

Fig. 1. Schönebeck WWTP configuration. Sampling points are indicated with white bubbles. Microbial samples were taken from the anaerobic tank in the secondary system (white bubble with microbe icon). Iron dosing points are indicated with red arrows (empty red arrow indicates extra dosing points compared to normal operation). During the chemP period, extra iron was dosed in the primary sludge.

et al., 2025), followed by analysis of variance to assess the global model adjusted R^2 and the marginal effects of Fe dosing and tank temperature (Z-score scaled). Centered log-ratio transformed read counts of core genera were calculated to overcome compositionality, facilitating correlational analysis with iron concentration in sludge and tank temperature. A reproducible workflow is made available on https://github.com/pietervanveelen/Nguyen_BioPtoChemP_mbio.

Potential shifts in the microbial community during the chemP operation were monitored, both at the general level and within specific bacterial groups of interest. The latter correlations are derived from clr-transformed microbial counts. The strength of relationships between microbial taxa and environmental parameters is expressed using Pearson correlation coefficients, where values close to 1 or −1 indicate strong positive or negative correlations, respectively.

Changes in microbial community composition do not occur immediately. Both chemical dosing and seasonal dynamics require time (due to a long SRT) to influence community composition. To capture these delayed responses, iron dosing and tank temperature were shifted forward in time relative to the microbial data. For each shift, the corresponding correlation was calculated, and the highest absolute value within a 12-week (one season) window was reported to indicate when each driver has had the strongest influence. Because iron dosing and seasonal temperature patterns are partly collinear, their effects are difficult to separate. Therefore, correlations with individual taxa should not be interpreted as independent effects of iron dosing alone, but as associations with the chemP operational period, during which iron concentration and temperature changed simultaneously.

3. Results and discussion

Schönebeck WWTP operated with biological phosphorus removal, with a low dose of iron at a molar ratio Fe/P of 0.5. To prepare the sludge for downstream magnetic vivianite recovery, additional iron was dosed into the primary thickener to promote vivianite formation in the sludge line and digester. We monitored the transition from bioP to chemP removal and the impact on vivianite formation over 8 months. The distribution of iron and phosphorus throughout the WWTP, as well as the effects of increased iron dosing on operational parameters and microbial communities were followed in detail. The timeline and naming of each phase are provided in Table 1.

Table 1
Different phases in the research project at Schönebeck WWTP.

BioP operation	ChemP operation	Return to bioP
Original operation with biological P removal	Increased iron dosing of original dosing points and extra iron dosed in primary sludge thickener	After extra iron dosing stopped, the WWTP returned to biological P removal (original operation)
05/04/2022 & 12/04/2022	13/04/2022 – 31/12/2022	01/01/2023 – 11/04/2023

3.1. Iron and phosphorus mass balance throughout the WWTP

Phosphorus and iron mass balances were established for two operational conditions of the WWTP: bioP and chemP. The bioP system was an established system before the tests, the mass balance for the bioP operation was therefore based on average flow and concentration measurements of 05/04/2022 and 12/04/2022, assuming these data represent the steady-state operation. Because only two detailed pre-dosing sampling events were available, this balance should be interpreted as a representative baseline snapshot rather than a complete statistical characterization of long-term bioP operation. For the chemP operation, data from the primary and secondary systems were averaged over the mid-October to mid-November period to account for the long retention time of the secondary system, while digester data were averaged from mid-November to mid-December, reflecting its own retention and the delayed feed of iron from upstream units. Due to lag-time effects and concentration fluctuations, the balances were not expected to close fully. The flows, concentrations, measured ranges, and indication of whether each flow was directly measured or calculated are provided in Supplementary Section S2.

The P mass balances are shown in Fig. 3. In both operations, the influent P load was similar, but there was significantly less phosphorus (4 kg/d) in the effluent with chemP. In theory, the difference between the influent and effluent P load should equal the P load in the dewatered sludge. Data from the digested sludge and dewatering centrate show that this sludge phosphorus load is 18 % lower with bioP and 8 % lower with chemP. These are considered acceptable differences for full-scale mass balances. Comparison of the bioP and chemP conditions highlighted two main differences in P flows within the plant.

The phosphorus load in the inlet of the primary thickened sludge during the chemP operation, unexpectedly, was lower than during bioP operation, with 23–32 kg/d (calculated values) for bioP compared to 8–20 kg/d (calculated values) for chemP. The extra iron addition in the thickener was expected to reduce phosphorus return via the thickener filtrate. It was also expected that a fraction of the added iron would be reduced to Fe^{2+} and recycled to the waterline. This was thought to result in higher P-removal by precipitation in the primary clarifier. However, the removal in the primary clarifier did not increase.

During chemP operation, a major change was observed in the phosphorus load in the centrate from the dewatering unit: 56 kg P/d during bioP compared to only 6 kg P/d under chemP. During bioP operation, phosphorus, accumulated as polyphosphate in the biomass, was released during anaerobic digestion and recycled to the water line.

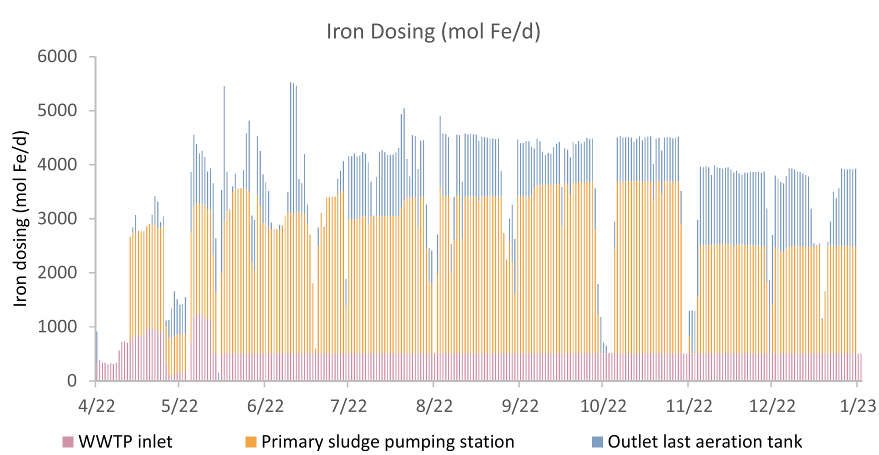

Fig. 2. Iron dosing during the test period from April-December 2022 to the Schönebeck WWTP. The amount added at different locations (Fig. 1) is indicated.

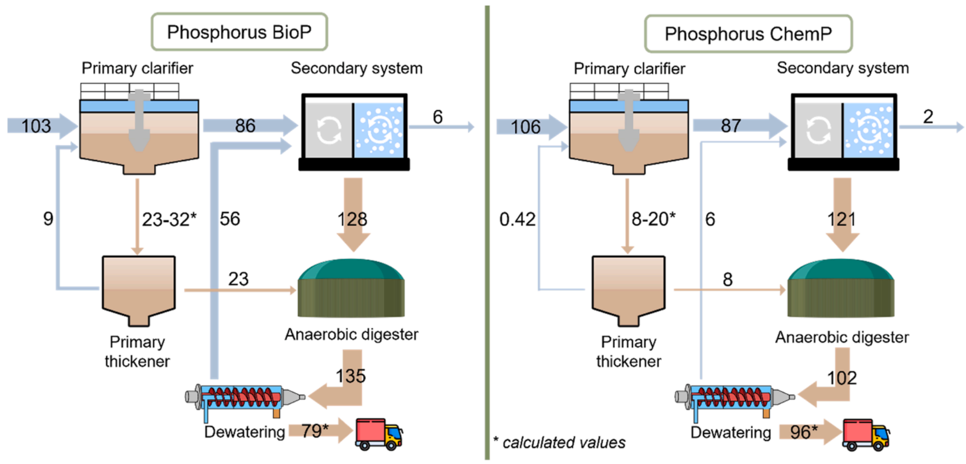

Fig. 3. Mass balance of phosphorus (kg/d) throughout the WWTP before (05/04/2022 and 12/04/2022) and near the end of the increased iron dosing period (12/12/2022). The value of each arrow shows the mass flow (kg P/day). The phosphorus load to the primary thickener inlet was expressed as a range, calculated either from the difference between the primary clarifier influent and effluent or from the summed primary thickener outlet loads. The raw ranges of each load component used in the mass-balance calculations are provided in Supplementary Section S2.

After the switch to chemP, this return flow dropped substantially as expected, as P was bound to iron in the sludge.

The iron balances are presented in Fig. 4. Loads in the sludge line in the primary, secondary, and digested sludge added up, particularly under the bioP operation. In the chemP operation, the digester received 321 kg/d and 289 kg/d was observed in the outlet. The lower value found in the digester outlet could be due to the digester not yet reaching full steady state during the increased iron dosing period. These results indicate that sludge line data are more reliable because the mass balances closed relatively well compared to those for the waterline. Partly, this can be due to sludge sampling being less affected by short-term flow and concentration fluctuations due to longer residence times.

Influent and primary clarifier effluent iron concentrations and loads over the waterline showed significant variability. In the waterline of a municipal WWTP, particulate iron is included in total iron measurements, but it is difficult to sample representatively because it is associated with suspended solids and flocs that are heterogeneously distributed and affected by local settling and resuspension. This likely contributed to the high variability in the measured waterline iron loads. Moreover, phosphorus is also partly present as particulate matter, and this may explain partly the discrepancies in the P balance discussed earlier.

For this reason, sludge line iron and phosphorus loads were used as the reference. The influent iron load was calculated as the difference between the dewatered sludge load and the total dosed iron, while the iron at the primary effluent was calculated as the difference between secondary thickened sludge and the iron dosed in the secondary clarifier. For the thickener return flows, most of the iron was present as soluble Fe^{2+}, which is less prone to underestimation This value was therefore used directly from measurement.

In the bioP operation, approximately 28 kg/d of iron was dosed in the influent of the primary clarifier, while around 25–27 kg/d (calculated values) was seen in the thickened primary sludge inlet. Based on the calculated iron balance, a fraction of the dosed iron enhanced coagulation in the primary clarifier and promoted phosphate binding in the primary thickener. However, a substantial portion of the influent iron appeared to remain soluble as Fe^{2+} or colloidal, limiting its removal in the primary clarifier and allowing it to pass to the secondary

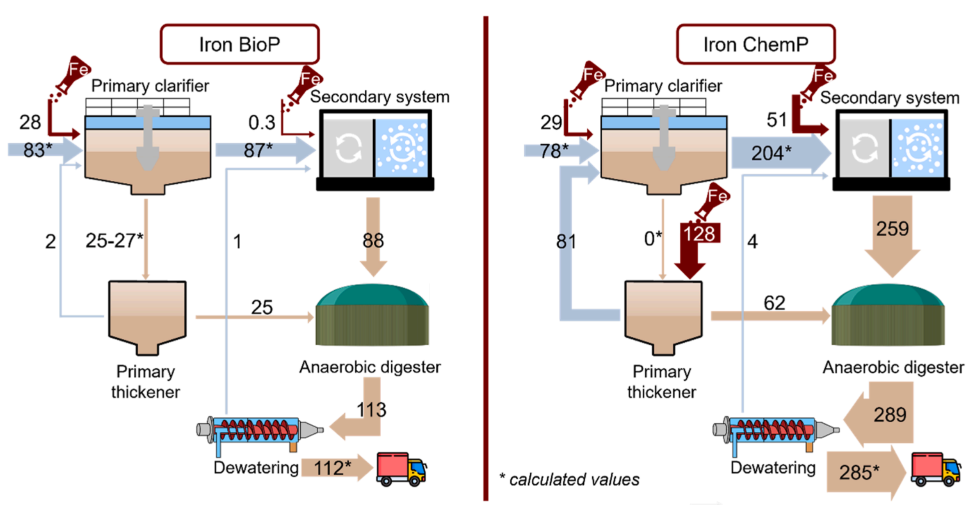

Fig. 4. Mass balance of iron (kg/d) throughout the WWTP before (05/04/2022 and 12/04/2022) and near the end of the increased iron dosing period (12/12/2022). The value of each arrow shows the mass flow (kg Fe/day). The iron load to the primary thickener inlet was expressed as a range, calculated either from the difference between the primary clarifier influent and effluent or from the summed primary thickener outlet loads. The raw ranges of each load component used in the mass-balance calculations are provided in Supplementary Section S2.

treatment. This iron then accumulated in the secondary sludge, making it the largest iron load entering the digester.

In the chemP operation, when 128 kg/d of iron was dosed in the primary thickener, the iron load in the primary thickened sludge did increase (from 25 to 62 kg/d). A significant amount of Fe appeared to recirculate from the primary thickener back to the waterline, more specifically to the primary settler (from 2 kg/d with bioP to 81 kg/d with chemP). Measurements showed that on average, 84 % of the recirculated Fe was in the reduced Fe^{2+} form, indicating reduction of dosed Fe^{3+} to Fe^{2+} with solubilization and transport with the supernatant. With an iron reduction rate of 0.05–0.06 h^{-1} and a residence time of almost 2 days in the thickener, it is possible that 90 % of the Fe^{3+} present could be reduced to Fe^{2+} (Prot et al., 2022; Wang et al., 2019). The reduction rate in primary sludge could even be higher than in activated sludge, as it has higher content of degradable organics and hence lower ORP favor Fe^{3+} reduction (Wang et al., 2019). Moreover, iron reducing bacteria could be present in the influent due to activity of these bacteria in sewer systems (Zhang et al., 2023). The soluble Fe^{2+} returned with the thickener return flow likely bypassed the primary clarifier. Despite the presence of Fe^{2+} in the primary clarifier, more phosphorus precipitation in primary sludge was not observed. In the bioP operation, higher phosphorus removal was associated with a greater availability of ferric iron in the primary clarifier which promotes the formation of iron(III) phosphate precipitates and iron hydroxides, thereby enhancing particulate P capture and flocculation and improving settling in the primary clarifier. In contrast, during chemP operation, recycled iron was predominantly ferrous, which is less effective for immediate P precipitation (Kemira Oyj, 2024). Although Fe^{2+} can bind phosphate via vivianite formation under anaerobic conditions, freshly formed vivianite may not be efficiently retained in the primary clarifier. Vivianite nucleates rapidly (Paskin, 2024) and therefore results in many small crystals which are difficult to fully separate in a primary clarification process. Consequently, secondary sludge became the main carrier of iron to the digester, despite Fe^{3+} dosing to the primary sludge. Although the bioP balance was based on only two pre-dosing sampling days and therefore does not capture the full long-term variability of normal operation, the additional iron input during chemP operation was much higher than during bioP operation. Therefore, the interpretation that substantial iron reduction, recirculation, and Fe accumulation in the secondary sludge occurred during chemP operation is not expected to depend strongly on the exact bioP baseline.

Due to the complex circulation of iron and build-up of iron mass in the various sludge types, iron concentrations in the digester can only stabilize after iron levels in the secondary system reached steady-state, approximately four months after dosing began (Fig. 5). This time is equivalent to about four times the activated sludge SRT. This delayed stabilization aligns with observations from full-scale systems, where steady state typically occurs after approximately 3 SRTs. Following the end of increased iron dosing, secondary sludge iron concentrations took

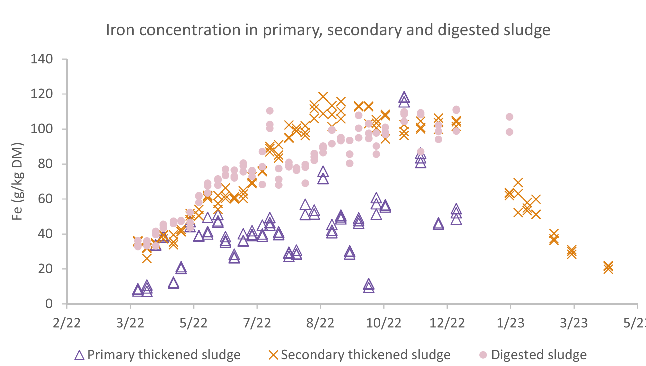

Fig. 5. Iron concentrations in the various sludges during the testing period at WWTP between 05/04/2022 and 11/04/2023. The increased iron dosing to promote vivianite formation ranged from 13/04/2022 until 31/12/2022.

roughly three months to return to the baseline (Fig. 5), highlighting the impact of SRT on the dynamics of iron in the system.

The optimal Fe/P ratio is plant-specific and depends on whether the goal is conventional P removal or vivianite recovery. Conventional chemical P removal can usually be achieved at lower Fe/P ratios, although increasingly strict effluent limits may require higher Fe/P ratios. Vivianite formation requires an Fe/P molar ratio close to 1.5, with additional iron potentially needed to compensate for Fe binding to sulphide. A more balanced strategy could therefore be evaluated, in which waterline dosing is maintained for P removal, while the additional iron required for vivianite formation is dosed into the digester.

In summary, the shift from bioP to chemP significantly changed the phosphate and iron mass flows in the Schönebeck WWTP. Phosphorus in the return water from the thickeners and dewatering unit decreased, due to better fixation of phosphate in the iron-rich sludge. A large fraction of the iron in the primary thickener was reduced, solubilised and recirculated to the waterline. For future implementation, a two-point dosing strategy may be considered as a process implication of this study. In this approach, waterline iron dosing would be maintained for effluent P control, while only the additional iron required to maximize vivianite formation would be dosed directly into the digester. Compared to primary sludge-line dosing, this could keep the additional iron in the sludge stream where vivianite formation and recovery are targeted, thereby reducing unnecessary iron recirculation through the rest of the plant and avoiding the long delay caused by iron accumulation in the secondary sludge before reaching the digester. Direct digester dosing was not tested in this study and should therefore be regarded as a strategy for further testing rather than a demonstrated solution. A potential risk is sludge acidification when high doses of acidic iron salts are applied, which could make conditions less favorable for vivianite formation and alter sludge characteristics. Alternative iron sources, such as ferric-based drinking water treatment sludge, could also be explored. Salehin et al. (2020) showed that ferric-based drinking water sludge could still form vivianite in downstream anaerobic digestion. Such solid iron sources may reduce the risk of acidification compared to liquid iron salts, but their effects on vivianite formation and recovery require further study. In addition, iron sulphate dosing should be avoided because additional sulphur input can increase sulphide formation, which competes with phosphate for iron binding, thereby limiting vivianite formation (Heinrich et al., 2023).

3.2. *Vivianite evolution in sludge*

During the test period, the vivianite formation in the digester and the amount of vivianite in the sludge were followed. Vivianite and all Fe-bound minerals were measured using Mössbauer spectroscopy, the fitting of the Mössbauer spectra is described in supplementary section S1.

The vivianite concentrations in primary and secondary thickened sludge collected on the final sampling day of the extra iron dosing period are reported in Table 2. In the primary sludge, 57 % of the iron was present as vivianite. This was despite the high iron dose and the strong

Table 2
Vivianite concentrations in primary and secondary thickened sludge on 12/12/2022 (last sampling day of increased iron dosing).

Sludge type	%Fe in vivianite	%P in vivianite	Fe/P molar	g vivianite/kg DM	Mass vivianite to digester (kg/d)
Primary thickened sludge	57	100	3.3	88	61
Secondary thickened sludge	92	85	1.4	284	910

reduction of iron to Fe^{2+} (Section 3.1), which would normally promote full vivianite formation. The main limiting factor was the low phosphorus content, since less phosphorus than originally anticipated was present in the primary sludge (Fig. 3). Based on our measurements of iron and phosphorus, the available phosphorus in the primary sludge was fully bound as vivianite.

In the secondary sludge, the vivianite concentration and the share of iron present as vivianite were 3.2 times and 1.6 times as high as in the primary sludge, respectively. The amount of phosphorus was larger and approximately 85 % of phosphorus was present as vivianite. The presence of vivianite in both primary and secondary thickened sludge agrees with similar observations reported by Amin et al. (2024) and Prot et al. (2022). These findings suggest that vivianite can already form in the primary thickener and secondary clarifier where iron reducing conditions occur. Formation in the secondary thickener is possible. However, the residence time there is minimal. Therefore, it is assumed that vivianite already existed before that in the secondary system.

The Mössbauer measurements of the last sampling day primary and secondary thickened sludge showed that vivianite was already present before anaerobic digestion. Since digested sludge solids were not recycled to the primary or secondary sludge lines, this vivianite could not have originated from the digester. This indicates that vivianite formation occurred upstream of the digester, particularly in the secondary sludge line, where suitable local conditions must have existed. Formation may have taken place in anoxic zones of the secondary treatment system or in anaerobic micro-environments. However, because detailed time-resolved measurements of ORP, Fe^{2+}, phosphate, and sulphide were not available for all upstream locations, and upstream sludge samples were only analyzed at the end of the dosing period, the timing and extent of upstream formation over the full campaign cannot be quantified. This differs from the findings of Amin et al. (2024) who observed increases in vivianite during digestion even though some had formed in the mixed sludge. However, vivianite formation can be plant-specific and depends on factors such as anaerobic retention time, process configuration, and Fe and P circulation within the system. These results suggest that, under suitable reducing conditions and sufficient sludge retention time, vivianite formation can occur without the need for anaerobic digestion, similar to the report by Prot et al. (2022).

The fractionation of iron as vivianite, iron-sulphides, or present in other forms in digested sludge was estimated from Mössbauer spectroscopy (Fig. 6). The "Fe in others" group refers to iron in phyllosilicates or metallic iron (section S1). In the bioP operation (05/04/2022), no vivianite was detected and a larger share of Fe was associated with S, which aligns with the preference of Fe to bind to S rather than P. After extra iron dosing, the amount of vivianite increased quickly, and the share of P present as vivianite in the digester rose from 0 % before dosing to about 90 % in mid-December. The iron addition was increased from an Fe/P ratio of 0.5 to 1.6 in the chemP operation, resulting in vivianite

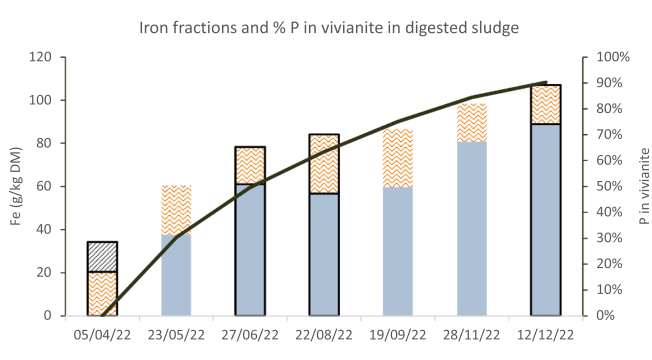

Fig. 6. Iron fractions in digested sludge through time, determined with Mössbauer spectroscopy. Samples with black borders were measured at 4.2 K. The rest were measured at room temperature.

formation.

Iron addition substantially improved biogas quality, reducing the H_2S concentration from 332 ppm in January 2022 to 1 ppm in January 2023, indicating that Fe immobilized S in the sludge. However, the amount of Fe bound to S remained largely unchanged when shifting from bioP to chemP, averaging 21 g Fe/kg DM. A rough mass balance shows that the reduction in H_2S corresponds to approximately 0.64 kg S/d, whereas the S content in digested sludge is about 49 kg S/d. Therefore, the S removed from the gas phase represents only a very small fraction of total sludge S, making changes in the Fe-bound S fraction difficult to detect in the sludge phase. Earlier work proposed that Fe^{2+} becomes available for vivianite only after all sulphide has bound Fe^{2+} at a 1:1 molar ratio (Prot et al., 2020). In our case, however, only 66 % ± 12 % of the S pool was Fe-bound in a 1:1 ratio regardless of the iron concentration in the digester. Differences from earlier findings may stem from operational and sludge characteristics: our digested sludge contains roughly twice the sulphur concentration reported by Prot et al. (2020) and Wilfert et al. (2018) (18.5 vs. 10 g S/kg DM), while Fe concentrations are comparable. Additionally, our sludge originates from EBPR systems shifted to CPR operation, whereas their studies focused mainly on CPR sludge, thus there could be differences in chemical composition and microbial activity. The constant S-bound Fe fraction despite increasing Fe dosing suggests that total sludge sulphur was not equivalent to sulphur available for Fe binding. However, sulphur speciation was not determined in this study, so the chemical nature of the remaining non-Fe-bound sulphur cannot be identified. Further work on sulphur speciation in bioP-derived sludge is needed to determine how this affects S competition for Fe and vivianite concentration prediction.

Overall, the results demonstrate that vivianite formation was enhanced with extra iron dosing. Moreover, vivianite was detected upstream of the digester, mainly from the secondary sludge. Iron dosing increased the fraction of phosphorus bound as vivianite in digested sludge to about 90 %, but Fe-S interactions were not stoichiometric. S-bound Fe fraction remained essentially constant despite increasing iron availability and accounted for only 66 % of the total sulphur pool.

3.3. *Impact of increased iron dosing on the operation of the WWTP*

This section explores the broader effects of increased iron dosing on WWTP performance beyond vivianite formation. The analysis focuses on how iron addition influenced sludge properties, particularly changes in dry matter content and their implications for biogas production. In addition, the effects on effluent quality and nitrogen removal are evaluated to assess whether the extra iron dosing introduced any unintended impacts on overall treatment efficiency.

3.3.1. *Sludge dry matter*

The loads of total and volatile solids from the primary and secondary thickener to the digester are reported in Fig. 7. During chemP operation, there was a gradual decrease in the DM and VS loads from the primary thickener (from around 2.6 ton/d of VS at the beginning to only 0.6 ton/d at the end of the period). This represents a significant drop of 77 % in primary sludge. The decrease in primary sludge TS and VS loads coincided with the high return of Fe^{2+} from the primary thickener to the waterline. This suggests that Fe^{2+} recirculation may have contributed to reduced primary solids capture, although the exact mechanisms cannot be confirmed because floc properties and primary settling kinetics were not directly measured. Apart from the increased iron dosing, no major intentional operational change was made in the primary treatment step, but seasonal variation in influent sludge characteristics cannot be excluded.

Iron dosing in wastewater treatment is often applied to enhance coagulation, improve sludge settleability, and aid in the removal of COD, TS, and VS (Asensi et al., 2019; Shrestha et al., 2019). The effectiveness of iron, however, depends on its oxidation state. Because most colloids in water carry negative charges, their destabilization depends

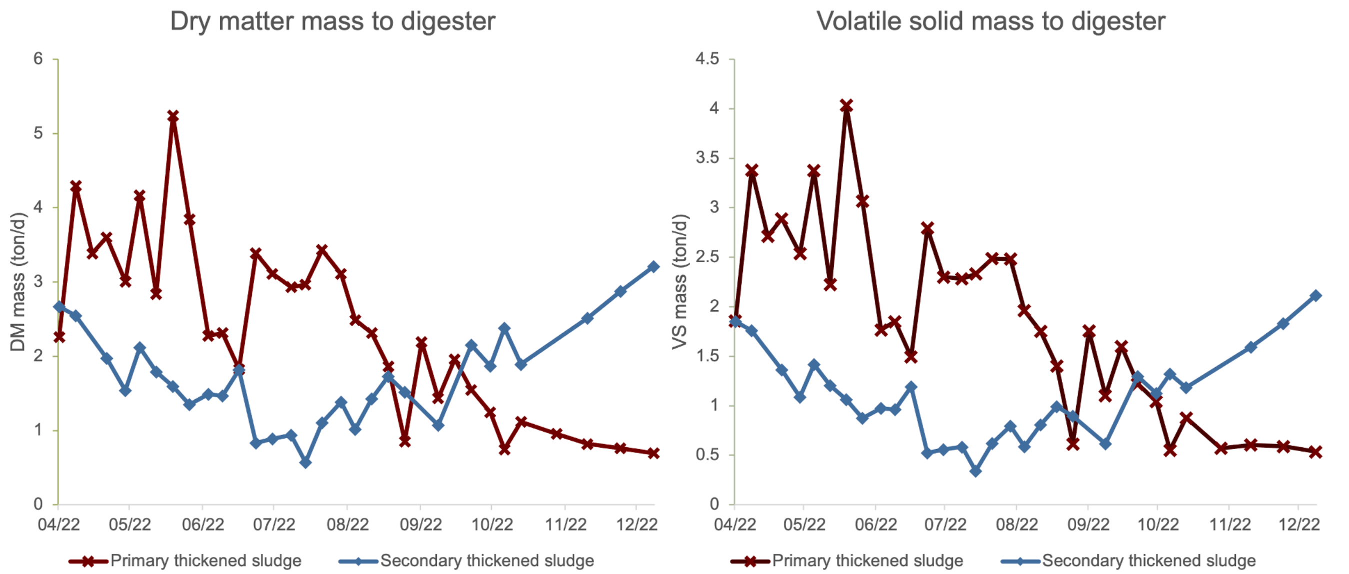

Fig. 7. Dry matter (or TS) (left) and volatile solid (right) loads to the digester of primary and secondary thickened sludge. The first 2 data points are the original bioP operation (05/04/2022 &12/04/2022).

on charge neutralization, and ferric iron (Fe^{3+}), having a higher positive charge than ferrous iron (Fe^{2+}), is more effective in promoting coagulation, leading to stronger floc formation and improved settleability of suspended solids (Duan and Gregory, 2003; Kemira Oyj, 2024). In our case, most of the iron recycled to the primary settler remained in the ferrous form. When Fe^{2+} is abundant and dominating like in the case of chemP, it might compete with Fe^{3+} for organic binding sites but forms weaker complexes, preventing Fe^{3+} from creating strong, cross-linked flocs, thus overall floc strength and settleability could decrease.

With the decrease in primary sludge production, it was expected that the secondary sludge production would increase. However, both TS and VS production in the secondary system also declined, dropping from VS of 1.8 ton/d at the start to 0.6 ton/d by mid-September. This reduction likely reflects the lower biomass yield during the warmer months. Elevated temperatures enhance microbial metabolism and endogenous respiration, leading to greater oxidation of organic matter to CO_2 (Tchobanoglous et al., 2014). Unlike the primary sludge, the secondary thickened sludge showed a turning point: from mid-September onward, its TS and VS production increased gradually. This aligns with decreasing temperatures and lower endogenous respiration rates. Moreover, at the end of August, the operators modified the process by lowering aeration in tank 2 to create an extra anoxic zone for improved denitrification. This change reduced VS oxidation, which may partly explain the subsequent increase in VS load in the secondary sludge to the digester. Although the lower primary sludge capture may have increased the organic load entering the secondary treatment, the system was already operated with excess aeration capacity before the reduced aeration, and effluent COD improved. Therefore, no reliable additional aeration energy or impact could be quantified from the available data.

Taken together, the reduced primary sedimentation efficiency, iron recirculation into the secondary treatment step, and delayed delivery of iron to the digester indicate that dosing all additional iron into the primary thickener is not the preferred strategy. Direct extra iron dosing in the digester would likely reduce Fe recirculation through the waterline and may reduce the risk of reduced primary solids capture if this was indeed linked to Fe^{2+} recirculation.

3.3.2. Sludge dewatering

The dry matter content of the dewatered sludge increased from 24 % to 30 % by the end of the dosing period, exceeding the values observed during both the bioP baseline and previous years of plant operation. Since polymer dosing and centrifuge operation remained within normal operational ranges, this improvement was likely linked to increased vivianite formation, which accounted for 26.6 wt% of the digested sludge dry matter at the end of the dosing period. Although the mass of dry matter in the sludge increased, the total annual sludge disposal mass remained comparable to previous years. This suggests that the additional dry matter was fully compensated by a reduction in water content in the dewatered sludge, resulting in unchanged disposal mass and indicating improved dewatering efficiency. This observation is consistent with literature reporting that sludge from bioP systems is more difficult to dewater than sludge from chemically precipitated systems (Shimp et al., 2013). It was suggested that the lower orthophosphate concentration in sludge may contribute to improved dewaterability (Bergmans et al., 2014). In the chemP operation, most phosphorus in the sludge was already bound to iron as vivianite (Fig. 6). In contrast, during the bioP operation, a substantial amount of phosphate was released in the digester due to PAOs activity under anaerobic conditions (Fig. 3). If magnetic recovery is applied and 80 % of vivianite is removed from the sludge, the sludge disposal volume could potentially be reduced by approximately 20 %, if removal of vivianite would not significantly impact the dewaterability. Therefore, improved dewaterability and potential vivianite removal could provide an operational cost benefit by reducing sludge disposal, while also contributing to phosphorus recovery targets through vivianite recovery. There are also additional operational effects of increased iron dosing and ViviMag® implementation at the same WWTP reported by Grönfors et al. (2022).

3.3.3. Effluent quality

Due to the increased iron dosing, the concentration of total P in the effluent decreased significantly, from an average of 1.3 mg/l to 0.2 mg/l, bringing the P concentration down to well below the new limits set for total effluent P (0.7 mg/l) (Directive (EU) 2024/3019, 2024), representing an 86 % reduction. Notably, a significant decline in effluent P was only observed starting in August (Figure S3), which coincided with the period when iron accumulation in the secondary treatment system reached its peak. This temporal pattern supports the observation that it took several months for iron to effectively reach and stabilize within the secondary system from Section 3.1. Similar to phosphorus, the total COD concentration in the effluent showed a decreasing trend over time, most strongly since the end of August, declining from 41 to 27 mg/l, a reduction of 34 %.

3.3.4. Nitrogen removal

Nitrate concentrations in the effluent showed considerable variation from May 2022 (Fig. 8), requiring improved denitrification to meet spot-sample regulations. In response, as mentioned above, at the end of August, the WWTP reduced aeration in the second out of the three nitrification tanks from 0.7 to 0.3 mgO_2/l, thereby making this tank possibly become a mix of nitrification and denitrification zone. According to the WWTP operators, 2/3 of the nitrification process happened already in the first tank. Following this conversion, effluent nitrate variability decreased. However, this improvement came at the expense of reduced nitrification capacity after a few weeks, as reflected by increasing effluent ammonia, though it was still within the limits.

3.4. Impact of chemP operation on the microbial dynamics

As described in the Methods, lagged Pearson correlations were used to account for delayed microbial responses to changes in operational conditions. Because iron dosing and seasonal temperature patterns were partly collinear, these correlations should be interpreted as temporal associations rather than independent causal effects.

While many bacteria share functional roles, we highlight taxa that showed the strongest variation, clear associations with iron, notable abundance, or established functional relevance. Since iron addition modifies chemical conditions and biological phosphorus removal processes, tracking microbial community structure helps identify taxa whose relative abundance was associated with the operational transition. Full-scale studies on long-term iron dosing remain limited, so this work offers new insight into how chemical dosing interacts with seasonal effects to shape microbial ecology in real WWTPs.

3.4.1. Overall microbial community shift

To explore the temporal dynamics in microbial community structure, a Constrained Analysis of Principal Coordinates (CAP) was performed (Fig. 9). This analysis relates community dissimilarities to environmental variables, in this case total iron concentration in thickened secondary sludge and tank temperature, to assess associations between microbial community structure, iron dosing, and seasonal effects. The CAP ordination revealed a clear temporal structure in the microbial community across the monitoring period. The two displayed CAP axes accounted for 63.2 % of the total constrained variance. It is important to note that this ordination uses the direct, unshifted (Z-score scaled) iron and tank temperature values. As discussed above, microbial responses often occur with a delay, so the influence of these drivers is likely captured only partly in the immediate correlations shown here.

In the CAP analysis, the early samples collected prior to the extra iron dosing clustered toward the left side of the CAP1 axis. With the start of increased iron dosing and the resulting increase in iron concentrations in the sludge line, subsequent samples shifted progressively along CAP1 toward the right, indicating a strong directional response of the microbial community to iron addition since the CAP1 axis aligned closely with the iron concentration vector. This suggests that iron concentration was one of the main variables associated with the observed shifts in community composition during this period. Temperature was oriented diagonally between CAP1 and CAP2, indicating that it contributed to variation on both axes.

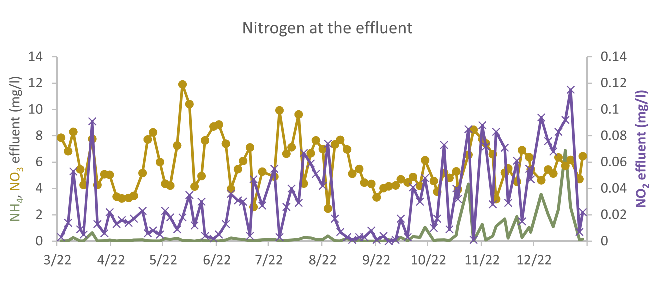

Fig. 8. Concentrations of ammonia, nitrite and nitrate at the WWTP effluent.

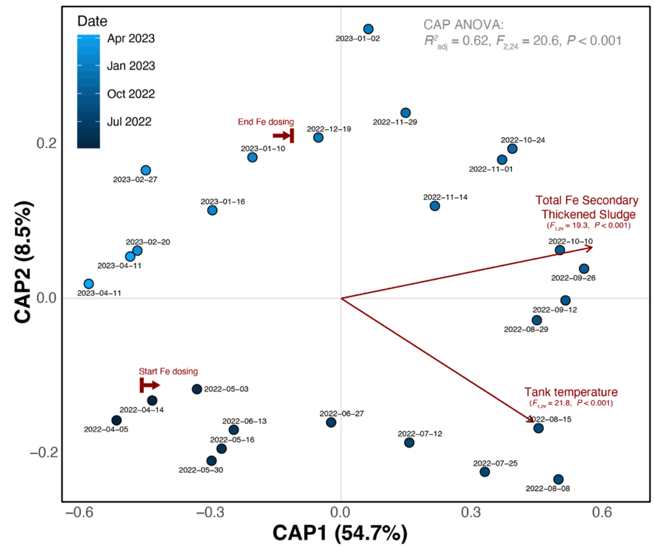

Fig. 9. Constrained Analysis of Principal Coordinates (CAP) of the microbial community through time. The two constraints are total iron concentration in the secondary thickened sludge and tank temperature.

After the end of extra iron dosing (beginning of 2023), the final 7 samples slowly shifted back along CAP1 toward the region occupied by the baseline, pre-dosing samples. By April 2023, the microbial core community composition had shifted back close to the April 2022 bioP position, although the overlap was not complete. This suggests substantial recovery toward the original bioP community after the temporary chemP period. Such recovery is possible because after additional iron dosing stopped, the plant returned to the same bioP operation and remained connected to the same sewer catchment. Recent work shows that the sewer microbiome is a major source of process-critical activated sludge taxa and can strongly shape activated sludge community assembly (Riisgaard-Jensen et al., 2025). Therefore, the return of the original operating conditions together with continued microbial input from the same sewer system likely supported re-establishment of the bioP-associated community. The residual difference may reflect stochastic temporal variation in incoming microbial pool and seasonal species-level dynamics in activated sludge (Peces et al., 2022; Riisgaard-Jensen et al., 2025). Since effluent P removal remained stable after the return to bioP operation, functional redundancy in the reassembled core microbial community may suggest that no loss of process stability was observed during the monitored period.

Overall, the CAP analysis indicates that microbial community composition was strongly associated with the extra iron dosing period, while the post-dosing samples showed a partial shift back toward the baseline bioP community structure. However, iron dosing and seasonal temperature were partly collinear during the monitoring period. This collinearity limits attribution of specific microbial shifts to iron dosing alone, especially for taxa that also showed strong lagged correlations with temperature.

To better understand how the microbial community changed during the sampling, Fig. 10 presents the temporal shifts in the relative abundance of the core microbial genera. The bacteria with the highest abundances and most prominent changes during extra iron dosing period will be analyzed in this section.

The most pronounced change was observed in *Candidatus Microthrix*, a filamentous bacterium known for its role in sludge bulking and foaming in WWTPs. Prior to the increased iron dosing, *Microthrix* constituted over 40 % of the core microbial community. Its abundance declined sharply to 0.6 % by the end of September, coinciding with the

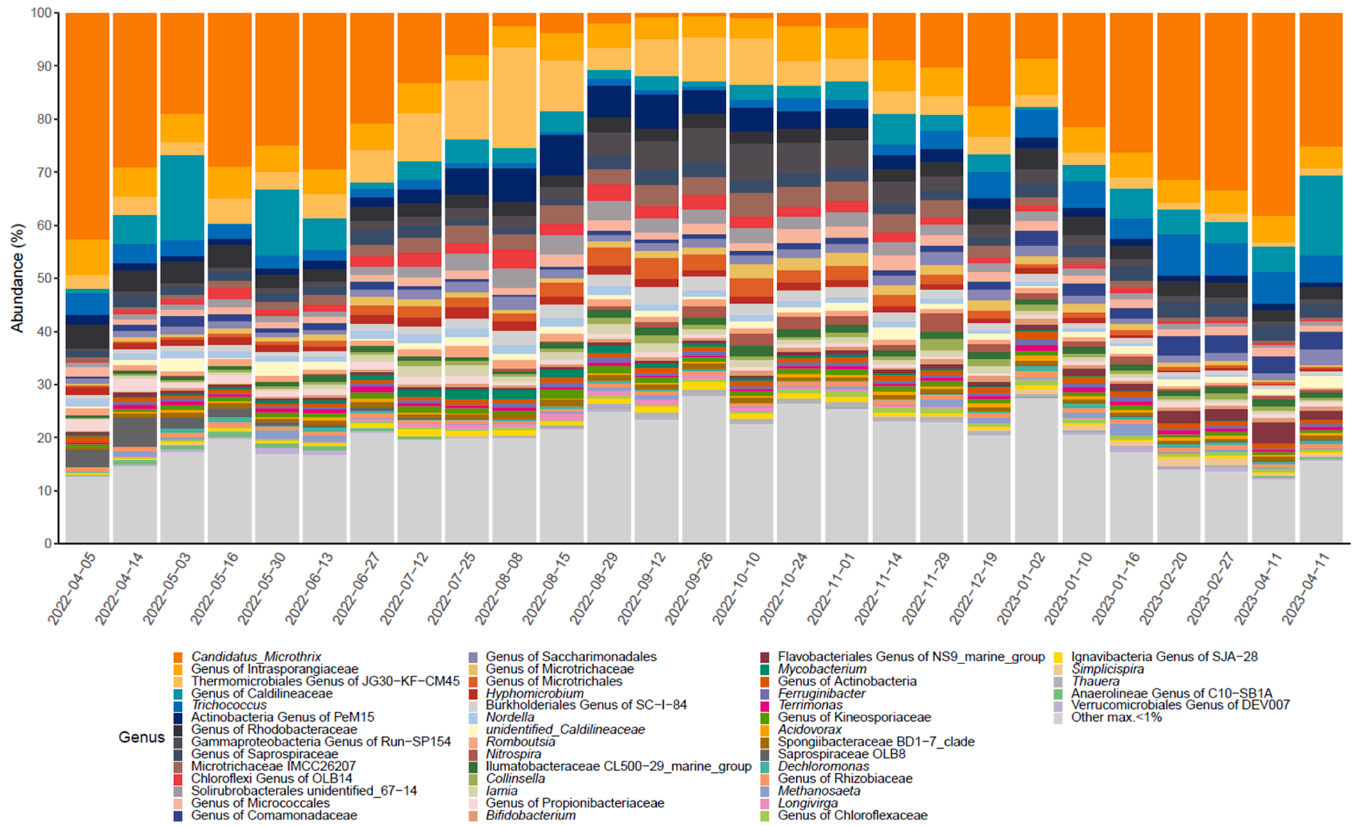

Fig. 10. Relative abundance of microbial community through time.

peak of iron concentrations in the secondary thickened sludge. Following the stop of the extra iron dosing, *Microthrix* became more represented again in the core community. The clr-transformed counts of *Microthrix* showed a strong direct negative correlation with iron concentrations (r = −0.88). This observation aligns with prior studies that demonstrated the inhibitory effect of iron salts on *Microthrix* and their potential to mitigate foaming and bulking (Knaf et al., 2013; Mamais et al., 2011). In addition, it also displayed a high negative correlation with temperature at an 8-week shift (r = −0.94), suggesting that seasonal conditions may have contributed as well. This is consistent with studies showing that *Microthrix* thrives in colder periods such as winter and spring and grows slowly, which supports the observed lag response (Peces et al., 2022). Along with this, the sludge volume index (SVI) values decreased (from 110 to 75 ml/g), indicating better settleability, coinciding with when *Microthrix* was absent (r = 0.83). After the extra dosing finished, the SVIs increased again.

Additionally, an unclassified genus of *Intrasporangiaceae* was the second most abundant group and showed a strong negative correlation with iron concentration (r = −0.82 at 1 week lag). A strong correlation with tank temperature at 8 weeks lag was also observed (r = −0.76). Members of this diverse family may contribute to phosphorus removal from wastewater (Stackebrandt et al., 2014).

Trichococcus, another genus with abundance change, showed a negative correlation between its clr-transformed counts and immediate iron concentration (r = −0.79) and temperature at 5 weeks lag (r = −0.93). Its relative abundance was initially around 3.6 % but decreased to below 1 % by late September, before recovering after extra dosing stopped. This response contrasts with results from constructed wetlands, where *Trichococcus* was reported to reduce with lower Fe^{3+} to Fe^{2+} concentration and was positively stimulated by increasing iron concentrations with maximum abundance (45.9 %) at 20 mg/l of iron (Tian et al., 2022). In our case, seasonal effects may have contributed to its lower abundance in addition to iron dosing since they were known to thrive in colder winter months (Peces et al., 2022). Notably, *Trichococcus* is known as a sludge bulking bacterium (Wang et al., 2016), and its clr-transformed counts correlate also strongly with sludge SVI (r = 0.92). Other microbial taxa in the WWTP were either present at low abundances in the WWTP or did not exhibit significant changes during high iron dosing.

3.4.2. PAOs and GAOs

As shown in Fig. 11, PAOs, including *Tetrasphaera, Dechloromonas*, and *Accumulibacter*, maintained relatively stable clr-transformed counts throughout the experiment. *Accumulibacter* was initially undetected in the community but was detected shortly after the increased iron dosing started. Its clr-transformed counts increased steadily, reaching approximately 1.4 during the high iron period, indicating that it became one of the more dominant taxa relative to the taxa geometric mean of the microbial population. *Accumulibacter* had a persistence of high clr (up to 2.3 by April 2023) values after iron concentrations declined.

Another common PAO which is *Phosphoribacter* was not found in this WWTP. After the dosing period ended, the WWTP continued to perform well, maintaining effluent P concentrations within permissible limits (Figure S3). This suggests that the good P removal was not due to residual iron, as iron levels in the secondary system had already returned to their low, pre-dosing (bioP) conditions, and that the temporary iron dosing did not cause substantial harm to PAOs.

Glycogen-accumulating organisms (GAOs), which are often considered competitors to PAOs (Oehmen et al., 2007) showed similar trends to PAOs, as illustrated in Fig. 11. GAOs generally had lower compositional balances than PAOs, suggesting that GAOs did not dominate the monitored core community under iron-rich conditions. *Contendobacter* and *Defluviicoccus* showed no clear temporal compositional balance shift, while the balance of *Competibacter* increased during and after the extra iron dosing period.

Iron dosing was expected to reduce the availability of phosphate for

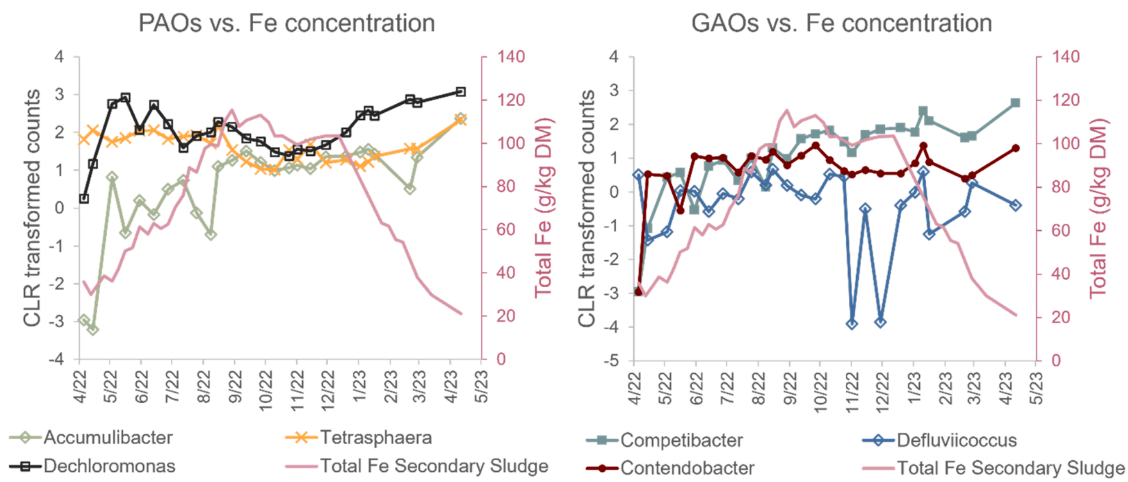

Fig. 11. Clr-transformed counts for PAOs (left) and GAOs (right) in the anaerobic tank vs. iron concentration in secondary thickened sludge.

PAOs, potentially suppressing their populations while favoring the growth of GAOs (Xia et al., 2022). However, findings in the literature remain inconsistent. For example, Yilmaz et al. (2017) reported that iron dosing could actually enrich *Accumulibacter*. Supporting this, Welles et al. (2016) demonstrated that both *Accumulibacter* and *Competibacter* are capable of growth under phosphate-limiting conditions, which is consistent with the continued detection of these genera in our 16S dataset. Previous studies have suggested that, under low-phosphate conditions, PAOs may rely more strongly on glycogen-associated metabolism (Hong et al., 2024; Welles et al., 2015; Zhou et al., 2008). In line with this adaptive resilience, Wang et al. (2020) showed that after aluminium sulphate dosing stopped, bioP activity and polyphosphate-accumulating metabolism recovered. In our study, the post-dosing effluent P performance and the continued detection of PAO-associated genera are consistent with recovery of bioP performance, although PAO activity and polyphosphate metabolism were not directly measured.

Overall, the 16S community profiles indicate that PAOs persisted during the extra iron dosing period and remained detectable after bioP operation resumed. However, because no activity tests were performed, potential shifts in PAOs' metabolism cannot be confirmed. The coexistence and apparent stability of PAOs and GAOs suggest that temporary chemP operation did not lead to clear GAOs dominance or a persistent loss of PAOs.

3.4.3. Iron-related microbes

Iron-cycling microorganisms such as *Leptothrix* and *Geothrix* had a positive compositional balance shift in parallel with rising iron concentrations (Fig. 12). *Leptothrix*, known for its role in Fe^{2+} oxidation, and *Geothrix*, a dissimilatory Fe^{3+}-reducing bacterium both showed strong positive correlations immediately with iron levels ($r = 0.80$ and $r = 0.75$, respectively). Their negative log-ratio shift after the additional iron dosing stopped further suggest that they were more represented when iron availability in the sludge environment was higher (Berg et al., 2019; Seguel Suazo et al., 2025).

Other known iron oxidizers such as *Gallionella* and *Sphaerotilus* and iron reducers like *Geobacter, Shewanella* and *Desulfovibrio*, etc. were also investigated. However, either they were not found in our samples, or did not experience significant alteration due to the extra iron dosing.

3.4.4. Nitrifiers and denitrifiers

Fig. 13 shows the shifts in nitrifiers and denitrifiers before and after the extra iron dosing period. The clr-transformed counts of *Nitrosomonas* (an ammonia-oxidizing bacterium, AOB) remained relatively stable across the sampling period, showing highest correlation with iron concentration at 9 weeks lag ($r = -0.81$) and no significant correlation with temperature throughout the 12-week lag. *Nitrospira*, a nitrite-oxidizing bacterium (NOB), even though exhibited delayed correlation with iron ($r = 0.83$ at 10 weeks lag), showed a positive compositional balance shift from September 2022. However, even after the extra iron dosing stopped, these microbes remained detectable in the 16S profiles. The positive compositional balance shift of *Nitrospira* is unexpected given the reduction in the aerated zone since end August (Section 3.3.4), as these organisms require oxygen to survive. However, since 2/3 of the nitrification had already occurred in tank 1, the reduced aeration in tank 2 likely had a limited impact on their population. Additionally, other nitrifying bacteria present in the WWTP might have contributed more significantly to nitrite removal and could therefore be the main drivers

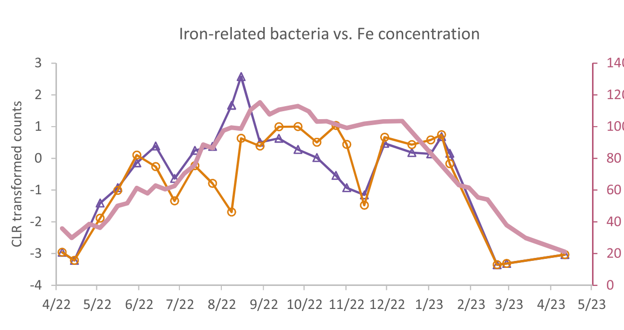

Fig. 12. Clr-transformed counts for iron reducing bacteria Geothrix and iron oxidizing bacteria Leptothrix in the anaerobic tank vs. iron concentration in secondary thickened sludge.

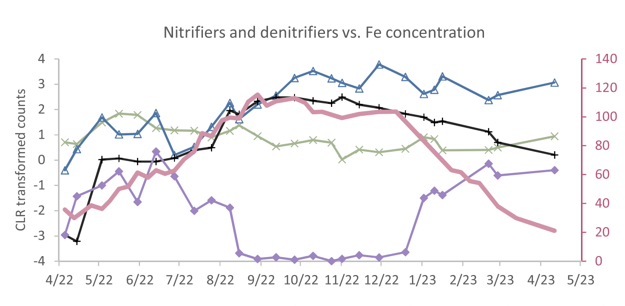

Fig. 13. Clr-transformed counts for nitrifiers (Nitrosomonas and Nitrospira) and denitrifiers (Thauera and Zoogloea) in the anaerobic tank vs. iron concentration in secondary thickened sludge.

of the observed results. Previous studies have also reported that iron addition can enhance the population of *Nitrospira* (Yang et al., 2020; Yilmaz et al., 2017).

In contrast to nitrifiers, the denitrifying community showed a stronger response to iron addition. *Thauera*, a well-known denitrifying genus, showed a highly positive log-ratio shift during the high iron dosing period, with a strong positive correlation to iron ($r = 0.94$ at 3 weeks lag). Their correlation with temperature peaked at 12 weeks lag ($r = 0.92$). This genus is commonly found in denitrifying environments and is known for its metabolic flexibility, including the use of aromatic compounds and iron-coupled electron transport (Yang et al., 2020). Supporting evidence from Wang et al. (2019) indicates that iron addition can promote *Thauera*, with their work reporting higher relative abundances were observed in CPR sludge compared to EBPR sludge (2.5 % vs 0.9 %), with an increase from 2.5 % to 3.5 % following iron dosing, whereas only a minor decrease was reported in EBPR sludge (from 0.91 % to 0.68 %). Moreover, the increase in denitrification zone between the end of August to the end of November in the biological tank 2 could also contribute to the growth of *Thauera*.

Zoogloea, another denitrifier associated with floc formation and EPS production, showed negative compositional balance shift after June and was only weakly detected during the period of peak iron concentrations. Its abundance began to recover only after the extra iron dosing was stopped in early 2023. *Zoogloea* abundance was negatively correlated with iron ($r = -0.85$ at 1 week shift) and negatively correlated to tank temperature ($r = -0.91$ at 9 weeks lag). *Zoogloea* was also considered to be abundant in systems where iron was present (Chen et al., 2023), contrary to our findings. However, because *Zoogloea* was already weakly represented compared with *Thauera* at baseline, this temporal pattern should be interpreted cautiously in relation to overall denitrification performance.

Since many bacteria can contribute to denitrification and the presence of iron can influence which denitrification species are favored, identifying the exact contributors is difficult. Although spikes in effluent nitrate concentrations were likely caused by operational issues at the WWTP, leading to increasing the denitrification zone, the denitrification process remained effective, as seen from the stabilized NO_3 concentration in the effluent, as discussed in Section 3.3.4. Even after the additional iron dosing stopped, and higher aeration resumed in the extended denitrification tank since the end of November 2022, no observable impact was seen on the denitrification process and on denitrifier *Thauera*, suggesting that iron did not have a negative impact on denitrification.

Overall, microbial community composition showed clear shifts during the extra iron dosing period. Filamentous bacteria, particularly Microthrix, had a negative compositional balance shift in the 16S profiles, while PAOs and GAOs showed no clear shift toward GAOs dominance and PAOs remained detectable throughout the monitoring period. Iron-related bacteria, as well as nitrification- and denitrification-associated microbes, showed variable responses, but the overall nitrogen removal process remained unaffected. These observations are based on clr-transformed counts derived from 16S rRNA gene sequencing. Therefore, the results reflect changes in the representation of each genus relative to the geometric mean of the selected core community, not absolute cell numbers or microbial activity. Consequently, the observed patterns should be interpreted as associations with the chemP period, iron concentration, temperature, and operational conditions, rather than as direct evidence of population growth or functional activity. Furthermore, once the extra iron dosing ended, the microbial community largely returned close to its original state, demonstrating its resilience.

4. Conclusion

Converting a WWTP with biological P removal to chemical P removal to enable vivianite production from digested sludge is technically feasible and reversible under the conditions of the study. By increasing iron dosing to an Fe/P molar ratio of 1.6, the proportion of P bound as vivianite in the digested sludge increased from 0 % to 90 %. This dose exceeds the requirement for chemical P removal but was needed to maximize vivianite formation.

With this high dose of iron, several operational advantages were observed: dewatering improved considerably, resulting in a 25 % increase in dry matter of the dewatered sludge and a corresponding reduction in water content. The concentration of H_2S in biogas dropped significantly from 332 ppm to 1 ppm. Effluent quality also improved with lower P (86 % reduction) and COD (34 % reduction) concentrations.

Iron dosing to primary sludge resulted in iron solubilization and accumulation in the secondary sludge. This slowed the accumulation in the digester. Therefore, future implementation could consider a two-point dosing strategy: conventional waterline dosing should be maintained for effluent P control, while the additional iron required for vivianite formation can be dosed directly to the digester.

Interestingly, the PAO community remained stable during the testing period, independent of the extra iron dosing. The other members of the microbial community showed shifts during the iron dosing period, when the additional dosing stopped, the community returned close to its original composition.

Declaration of generative AI and AI-assisted technologies in the writing process

The author(s) utilized ChatGPT to enhance the clarity and style of the manuscript. All content generated with this assistance was subsequently reviewed and revised by the authors, who accept full responsibility for the accuracy and integrity of the published work.

CRediT authorship contribution statement

Ha Nguyen: Conceptualization, Data curation, Formal analysis, Investigation, Methodology, Visualization, Writing – original draft, Writing – review & editing. **Leon Korving:** Conceptualization, Formal analysis, Methodology, Supervision, Writing – review & editing. **Thomas Prot:** Conceptualization, Formal analysis, Methodology, Supervision, Writing – review & editing. **Damien Cazalet:** Conceptualization, Data curation, Formal analysis, Methodology, Writing – review & editing. **H. Pieter J. van Veelen:** Data curation, Formal analysis, Writing – review & editing. **Samarpita Roy:** Conceptualization, Formal analysis, Investigation, Writing – review & editing. **Carlo Belloni:** Formal analysis, Writing – review & editing. **A. Iulian Dugulan:** Formal analysis, Investigation, Methodology. **Mark C.M. van Loosdrecht:** Conceptualization, Supervision, Writing – review & editing.

Declaration of competing interest

The authors declare that they have no known competing financial interests or personal relationships that could have appeared to influence the work reported in this paper.

Acknowledgement

This work was performed in the cooperation framework of Wetsus, European Centre of Excellence for Sustainable Water Technology (www.wetsus.nl). Wetsus is co-funded by the European Union (Horizon Europe, LIFE, Interreg and ERDF), the Province of Fryslân and the Dutch Government: Ministry of Economic Affairs (TTT, SBO & PPS-I/TKI Water Technology), Ministry of Education, Culture and Science (TTT & SBO) and Ministry of Infrastructure and Water Management (National Growth Fund - UPPWATER). The authors would like to thank the participants of the research theme “Phosphate Recovery” for the fruitful discussions and their financial support. Additionally, the authors would like to thank Markus Biegel, Anne Verdurmen, Bernd Modler, Mehdi Nodeh and Baharnaz Amini from Veolia for the help with sampling and analytical work.

Supplementary materials

Supplementary material associated with this article can be found, in the online version, at doi:10.1016/j.watres.2026.126510.

Data availability

Data will be made available on request.

References

AbfKlärV, 2017. Ordinance on the reorganization of sewage sludge utilization sewage sludge regulation. Ordinance on the Reorganization of Sewage Sludge Utilization Sewage Sludge Regulation. https://www.bmuv.de/GE2.

AbwasserentsorgungSchönebeck GmbH. (n.d.). Abwasserentsorgung Schönebeck. Retrieved May 20, 2026, from https://www.abs-schoenebeck.de/.

Amin, L., Al-Juboori, R.A., Lindroos, F., Bounouba, M., Blomberg, K., Viveros, M.L., Graan, M., Azimi, S., Lindén, J., Mikola, A., Spérandio, M., 2024. Tracking the formation potential of vivianite within the treatment train of full-scale wastewater treatment plants. Sci. Total Environ. 912, 169520. https://doi.org/10.1016/j.scitotenv.2023.169520.

Asensi, E., Zambrano, D., Alemany, E., Aguado, D., 2019. Effect of the addition of precipitated ferric chloride on the morphology and settling characteristics of activated sludge flocs. Sep. Purif. Technol. 227, 115711. https://doi.org/10.1016/j.seppur.2019.115711.

Berg, J.S., Jézéquel, D., Duverger, A., Lamy, D., Laberty-Robert, C., Miot, J., 2019. Microbial diversity involved in iron and cryptic sulfur cycling in the ferruginous, low-sulfate waters of Lake Pavin. PLoS One 14 (2), e0212787. https://doi.org/10.1371/journal.pone.0212787.

Bergmans, B.J.C., Veltman, A.M., van Loosdrecht, M.C.M., van Lier, J.B., Rietveld, L.C., 2014. Struvite formation for enhanced dewaterability of digested wastewater sludge. Env. Technol. 35 (5), 549–555. https://doi.org/10.1080/09593330.2013.837081.

Bolyen, E., Rideout, J.R., Dillon, M.R., Bokulich, N.A., Abnet, C.C., Al-Ghalith, G.A., Alexander, H., Alm, E.J., Arumugam, M., Asnicar, F., Bai, Y., Bisanz, J.E., Bittinger, K., Brejnrod, A., Brislawn, C.J., Brown, C.T., Callahan, B.J., Caraballo-Rodríguez, A.M., Chase, J., Caporaso, J.G., 2019. Reproducible, interactive, scalable and extensible microbiome data science using QIIME 2. Nat. Biotechnol. 37 (8), 852–857. https://doi.org/10.1038/s41587-019-0209-9.

Chen, S., Zhou, B., Chen, H., Yuan, R., 2023. Iron mediated autotrophic denitrification for low C/N ratio wastewater: a review. Env. Res. 216, 114687. https://doi.org/10.1016/j.envres.2022.114687.

Directive (EU) 2024/3019, 2024. The European Parliament and of the Council on Urban Wastewater Treatment (Recast), 2024/3019. https://eur-lex.europa.eu/legal-content/EN/TXT/?uri=CELEX:32024L3019.

Duan, J., Gregory, J., 2003. Coagulation by hydrolysing metal salts. Adv. Colloid Interface Sci. 100-102, 475–502. https://doi.org/10.1016/S0001-8686(02)00067-2.

Dueholm, M.K.D., Nierychlo, M., Andersen, K.S., Rudkjøbing, V., Knutsson, S., Albertsen, M., Nielsen, P.H., 2022. MiDAS 4: a global catalogue of full-length 16S rRNA gene sequences and taxonomy for studies of bacterial communities in wastewater treatment plants. Nat. Commun. 13 (1), 1908. https://doi.org/10.1038/s41467-022-29438-7.

Egle, L., Rechberger, H., Krampe, J., Zessner, M., 2016. Phosphorus recovery from municipal wastewater: an integrated comparative technological, environmental and economic assessment of P recovery technologies. Sci. Total Environ. 571, 522–542. https://doi.org/10.1016/j.scitotenv.2016.07.019.

Grönfors, O., Cazalet, D., Vuori, V., Nguyen, H., Prot, T., Haarala, A., & Hansen, B. (2022). *Experiences from phosphorus recovery trials with the ViviMag® technology*. 334–351.

Heinrich, L., Schmieder, P., Barjenbruch, M., Hupfer, M., 2023. Formation of vivianite in digested sludge and its controlling factors in municipal wastewater treatment. Sci. Total Environ. 854, 158663. https://doi.org/10.1016/j.scitotenv.2022.158663.

Hong, Y., Cheng, H., Huangfu, X., Li, L., He, Q., 2024. Inhibition of phosphorus removal performance in activated sludge by Fe(III) exposure: transitions in dominant metabolic pathways. Front. Microbiol. 15. https://doi.org/10.3389/fmicb.2024.1424938.

Kemira Oyj, 2024. About water treatment. Kemira Oyj. https://www.kemira.com/stories/water-handbook-2020/.

Klencsár, Z., 1997. Mössbauer spectrum analysis by Evolution Algorithm. Nucl. Instrum. Methods Phys. Res. B: Beam Interact. Mater. At. 129 (4), 527–533. https://doi.org/10.1016/S0168-583X(97)00314-5.

Knaf, T., Schade, M., Lemmer, H., Benz, R., 2013. Specific binding of aluminium and iron ions to a cation-selective cell wall channel of microthrix parvicella. Env. Microbiol. 15 (10), 2775–2786. https://doi.org/10.1111/1462-2920.12138.

Könemann, R., Lehrmann, F., Hochgürtel, H., 2024. Aktuelle preise sowie zukünftige kosten der klärschlammentsorgung. Korresp. Abwasser · Abfall 71 (10), 792.

Korving, L., Van Loosdrecht, M., Wilfert, P., 2019. Effect of iron on phosphate recovery from sewage sludge. In: Ohtake, H., Tsuneda, S. (Eds.), Phosphorus Recovery and Recycling. Springer, pp. 303–326. https://doi.org/10.1007/978-981-10-8031-9_21.

Mamais, D., Kalaitzi, E., Andreadakis, A., 2011. Foaming control in activated sludge treatment plants by coagulants addition. Glob. Nest J. 13, 237–245.

McMurdie, P.J., Holmes, S., 2013. Phyloseq: an R package for reproducible interactive analysis and graphics of microbiome census data. PLoS One 8 (4), e61217. https://doi.org/10.1371/journal.pone.0061217.

Nguyen, H., Prot, T., Wijdeveld, W., Korving, L., Dugulan, A.I., Brück, E., Haarala, A., van Loosdrecht, M.C.M., 2024. Robust magnetic vivianite recovery from digested sewage sludge: evaluating resilience to sludge dry matter and particle size variations. Water Res. 266, 122407. https://doi.org/10.1016/j.watres.2024.122407.

Oehmen, A., Lemos, P.C., Carvalho, G., Yuan, Z., Keller, J., Blackall, L.L., Reis, M.A.M., 2007. Advances in enhanced biological phosphorus removal: from micro to macro scale. Water Res. 41 (11), 2271–2300. https://doi.org/10.1016/j.watres.2007.02.030.

Oksanen, J., Simpson, G.L., Blanchet, F.G., Kindt, R., Legendre, P., Minchin, P.R., O'Hara, R.B., Solymos, P., Stevens, M.H.H., Szoecs, E., Wagner, H., Barbour, M., Bedward, M., Bolker, B., Borcard, D., Borman, T., Carvalho, G., Chirico, M., Caceres, M.D., Weedon, J., 2025. *Vegan: community ecology package* (Version 2.7-2) [Computer software]. https://cran.r-project.org/web/packages/vegan/index.html.

Paskin, A. (2024). *Nucleation, growth and transformation phenomena of Vivianite*. https://doi.org/10.17169/refubium-43936.

Peces, M., Dottorini, G., Nierychlo, M., Andersen, K.S., Dueholm, M.K.D., Nielsen, P.H., 2022. Microbial communities across activated sludge plants show recurring species-level seasonal patterns. ISME Commun. 2, 18. https://doi.org/10.1038/s43705-022-00098-4.

Prot, T., Pannekoek, W., Belloni, C., Dugulan, A.I., Hendrikx, R., Korving, L., van Loosdrecht, M.C.M., 2022. Efficient formation of vivianite without anaerobic digester: study in excess activated sludge. J. Environ. Chem. Eng. 10 (3), 107473. https://doi.org/10.1016/j.jece.2022.107473.

Prot, T., Wijdeveld, W., Eshun, L.E., Dugulan, A.I., Goubitz, K., Korving, L., Van Loosdrecht, M.C.M., 2020. Full-scale increased iron dosage to stimulate the formation of vivianite and its recovery from digested sewage sludge. Water Res. 182, 115911. https://doi.org/10.1016/j.watres.2020.115911.

Riisgaard-Jensen, M., Valença, R.M., Peces, M., Nielsen, P.H., 2025. Sewer microbiomes shape microbial community composition and dynamics of wastewater treatment plants. ISME J. 19 (1). https://doi.org/10.1093/ismejo/wraf213 wraf213.

Salehin, S., Rebosura, M., Keller, J., Gernjak, W., Donose, B.C., Yuan, Z., Pikaar, I., 2020. Recovery of in-sewer dosed iron from digested sludge at downstream treatment plants and its reuse potential. Water Res. 174, 115627. https://doi.org/10.1016/j.watres.2020.115627.

Seguel Suazo, K., Nierychlo, M., Kondrotaite, Z., Petriglieri, F., Peces, M., Singleton, C., Dries, J., Nielsen, P.H., 2025. Diversity and abundance of filamentous and non-filamentous "Leptothrix" in global wastewater treatment plants. Appl. Env. Microbiol. 91 (3), e01485. https://doi.org/10.1128/aem.01485-24. -24.

Shimp, G.F., Barnard, J.L., Bott, C.B., 2013. Seeking to understand and address the impacts of biological phosphorus removal on biosolids dewatering. In: https://www.accesswater.org/publications/proceedings/-282038/seeking-to-understand-and-address-the-impacts-of-biological-phosphorus-removal-on-biosolids-dewatering.

Shrestha, S., Sharma, K., Chen, Z., Yuan, Z., 2019. Unravelling the influences of sewer-dosed iron salts on activated sludge properties with implications on settleability, dewaterability and sludge rheology. Water Res. 167, 115089. https://doi.org/10.1016/j.watres.2019.115089.

Stackebrandt, E., Scheuner, C., Göker, M., Schumann, P., 2014. The family intrasporangiaceae. The Prokaryotes. Springer, Berlin, Heidelberg, pp. 397–424. https://doi.org/10.1007/978-3-642-30138-4_176.

Tchobanoglous, G., Stensel, D.H., Tsuchihashi, R., Burton, F., Abu-Orf, M., Bowden, G., Pfrang, W., 2014. Metcalf & Eddy, Inc. Wastewater engineering: Treatment and Resource Recovery, 5th Edition. McGraw-Hill Education.

Tian, L., Yan, B., Ou, Y., Liu, H., Cheng, L., Jiao, P., 2022. Effectiveness of exogenous Fe2 + on nutrient removal in gravel-based constructed wetlands. Int. J. Env. Res. Public Health 19 (3), 1475. https://doi.org/10.3390/ijerph19031475. Article.

van Loosdrecht, M.C.M., Hooijmans, C.M., Brdjanovic, D., Heijnen, J.J., 1997. Biological phosphate removal processes. Appl. Microbiol. Biotechnol. 48 (3), 289–296. https://doi.org/10.1007/s002530051052.

Wang, B., Jiao, E., Guo, Y., Zhang, L., Meng, Q., Zeng, W., Peng, Y., 2020. Investigation of the polyphosphate-accumulating organism population in the full-scale simultaneous chemical phosphorus removal system. Environ. Sci. Pollut. Res. 27 (30), 37877–37886. https://doi.org/10.1007/s11356-020-09912-9.

Wang, P., Yu, Z., Qi, R., Zhang, H., 2016. Detailed comparison of bacterial communities during seasonal sludge bulking in a municipal wastewater treatment plant. Water Res. 105, 157–166. https://doi.org/10.1016/j.watres.2016.08.050.

Wang, R., Wilfert, P., Dugulan, I., Goubitz, K., Korving, L., Witkamp, G.-J., van Loosdrecht, M.C.M, 2019. Fe(III) reduction and vivianite formation in activated sludge. Sep. Purif. Technol. 220, 126–135. https://doi.org/10.1016/j.seppur.2019.03.024.

Welles, L., Lopez-Vazquez, C.M., Hooijmans, C.M., van Loosdrecht, M.C.M., Brdjanovic, D., 2016. Prevalence of 'Candidatus Accumulibacter phosphatis' type II under phosphate limiting conditions. AMB Express 6, 44. https://doi.org/10.1186/s13568-016-0214-z.

Welles, L., Tian, W.D., Saad, S., Abbas, B., Lopez-Vazquez, C.M., Hooijmans, C.M., van Loosdrecht, M.C.M., Brdjanovic, D., 2015. *Accumulibacter* clades type I and II performing kinetically different glycogen-accumulating organisms metabolisms for anaerobic substrate uptake. Water Res. 83, 354–366. https://doi.org/10.1016/j.watres.2015.06.045.

Wijdeveld, W.K., Prot, T., Sudintas, G., Kuntke, P., Korving, L., Van Loosdrecht, M.C.M., 2022. Pilot-scale magnetic recovery of vivianite from digested sewage sludge. Water Res. 212, 118131. https://doi.org/10.1016/j.watres.2022.118131.

Wilfert, P., Dugulan, A.I., Goubitz, K., Korving, L., Witkamp, G.J., Van Loosdrecht, M.C. M, 2018. Vivianite as the main phosphate mineral in digested sewage sludge and its role for phosphate recovery. Water Res. 144, 312–321. https://doi.org/10.1016/j.watres.2018.07.020.
Wilfert, P., Kumar, P.S., Korving, L., Witkamp, G.-J., van Loosdrecht, M.C.M, 2015. The relevance of phosphorus and iron chemistry to the recovery of phosphorus from wastewater: a review. Env. Sci. Technol. 49 (16), 9400–9414. https://doi.org/10.1021/acs.est.5b00150.
Xia, W.-J., Wang, H., Yu, L.-Q., Li, G.-F., Xiong, J.-R., Zhu, X.-Y., Wang, X.-C., Zhang, J.-R., Huang, B.-C., Jin, R.-C., 2022. Coagulants put phosphate-accumulating organisms at a competitive disadvantage with glycogen-accumulating organisms in enhanced biological phosphorus removal system. Bioresour. Technol. 346, 126658. https://doi.org/10.1016/j.biortech.2021.126658.
Yang, H., Deng, L., Xiao, Y., Yang, H., Wang, H., Zheng, D., 2020. Construction of autotrophic nitrogen removal system based on zero-valent iron (ZVI): performance and mechanism. Water Sci. Technol. 82 (12), 2990–3002. https://doi.org/10.2166/wst.2020.544.
Yilmaz, G., Cetin, E., Bozkurt, U., Aleksanyan Magden, K., 2017. Effects of ferrous iron on the performance and microbial community in aerobic granular sludge in relation to nutrient removal. Biotechnol. Prog. 33 (3), 716–725. https://doi.org/10.1002/btpr.2456.
Zhang, J., Chen, Z., Liu, Y., Wei, W., Ni, B.-J., 2023. Iron-assisted bio-chemical processes in sewer systems: iron cycle and its role in sewer management. J. Clean Prod. 414, 137707. https://doi.org/10.1016/j.jclepro.2023.137707.
Zhou, Y., Pijuan, M., Zeng, R.J., Lu, H., Yuan, Z., 2008. Could polyphosphate-accumulating organisms (PAOs) be glycogen-accumulating organisms (GAOs)? Water Res. 42 (10), 2361–2368. https://doi.org/10.1016/j.watres.2008.01.003.